AGU PUBLICATIONS

Geophysical Research Letters

RESEARCH LETTER
10.1002/2015GL063776

Key Points:
- Largest, deepest, and strongest storms are shown with spaceborne radar
- Extreme events are rare but important in global water cycle

Correspondence to:
C. Liu,
chuntao.liu@tamucc.edu

Citation:
Liu, C., and E. J. Zipser (2015), The global distribution of largest, deepest, and most intense precipitation systems, *Geophys. Res. Lett.*, *42*, 3591–3595, doi:10.1002/2015GL063776.

Received 9 MAR 2015
Accepted 16 APR 2015
Accepted article online 21 APR 2015
Published online 7 MAY 2015

The global distribution of largest, deepest, and most intense precipitation systems

Chuntao Liu[1] and Edward J. Zipser[2]

[1]Department of Physical and Environmental Sciences, Texas A&M University at Corpus Christi, Corpus Christi, Texas, USA, [2]Department of Atmospheric Sciences, University of Utah, Salt Lake City, Utah, USA

Abstract By grouping the contiguous precipitating area detected by the precipitation radar on board the Global Precipitation Mission (GPM) core satellite, snapshots of precipitation systems are summarized as precipitation features (PFs), and their properties are cataloged from 1 year GPM observations. These PFs are categorized by their area and depth and convective intensity based on the 20 and 40 dBZ radar echo tops, respectively. The largest PFs are found mainly over ocean at the mid-high latitudes, especially over southern ocean. The deepest PFs are mainly over tropical land, the West Pacific Warm Pool, and the Great Plains of the United States and Argentina. The most convectively intense PFs are dominant over land regions, including midlatitude and high latitude. The zonal precipitation contribution from extremely large precipitation systems is greater in midlatitude and high latitude than in the tropics. These extreme precipitation systems are rare but contribute significantly to the global precipitation. It is important to include their impacts in global climate models to correctly describe the global water cycle.

1. Introduction

Precipitation systems with large horizontal extent or with deep and intense convection have a large impact on our society because they are an important contributor to the hydrologic cycle and related to natural disasters such as flooding and all forms of severe weather. Therefore, many studies have attempted to describe the extreme precipitation systems globally. As early as in the 1980s, the global distribution of intense storms was determined by using the strength of the ice scattering signal observed by passive microwave radiometers as a metric [*Spencer and Santek*, 1985; *Mohr and Zipser*, 1996] and by the amount of the observed lightning [*Orville and Henderson*, 1986]. After the launch of the Tropical Rainfall Measuring Mission (TRMM) satellite [*Kummerow et al*., 1998] in late 1997, with a global coverage of 36°S–36°N, the first spaceborne radar on board TRMM enabled many studies of precipitation systems in great detail over tropics and subtropics [*Nesbitt et al*., 2000; *Cecil et al*., 2005], as well as specific precipitation systems, such as monsoon convective systems [*Houze et al*., 2007], shallow precipitation [*Schumacher and Houze*, 2003; *Liu and Zipser* 2009], and intense storms [*Liu and Zipser*, 2005; *Zipser et al*., 2006]. However, global radar observations over midlatitude and high latitude were lacking until the launch of CloudSat [*Stephens et al*., 2002] in mid-2006. Nadir scanning CloudSat provides a two-dimensional, vertical curtain of reflectivity from clouds and precipitation hydrometeors and is a great tool to study the global distribution of clouds [e.g., *Mace et al*., 2007; *Wall et al*., 2013]. However, it does not give a full three-dimensional view of the precipitation systems and lacks diurnal sampling [*Liu et al*., 2008a]. A large portion of precipitation at low levels in deep intense convective regions cannot be observed due to attenuation at CloudSat's W-band frequency, in addition to the lack of diurnal sampling coverage [*Liu et al*., 2008a].

As the successor of TRMM, the Global Precipitation Mission is a joint multisatellite mission by NASA and Japanese Space Agency focusing on the survey of global precipitation [*Hou et al*., 2014]. The core satellite has a dual frequency radar and advanced passive microwave radiometers onboard and was successfully launched in late February 2014. The GPM core satellite has a non-sun-synchronous orbit between 65°S and 65°N, which covers the globe except the polar regions. As this is written, 1 year of quality-controlled observations have been collected by GPM since early March 2014. This provides the first opportunity to conduct a true global survey of extreme precipitation systems with enough samples from precipitation radar. The motivation of this work is to address the following questions:

1. Where are the largest, deepest, and strongest precipitation systems on Earth?

2. How important is the contribution of these extreme precipitation systems relative to the global precipitation budget?

To answer these questions, first, we define the precipitation features (PFs) using the GPM precipitation radar observations and retrievals. Then the extremely large, deep, and intense PFs are identified after categorizing PFs based on their properties. Last, the fractions of precipitation produced by these extreme PFs are estimated.

2. Data and Methods

The GPM Ku band radar has specifications close to that of the TRMM precipitation radar [*Hou et al.*, 2014] and slightly improved sensitivity, so some weaker rainfall can be detected with a higher confidence (Takayabu, personal communication). The precipitation rate is retrieved from near-surface radar reflectivity [*Seto et al.*, 2013]. Following the algorithm for defining precipitation feature (PF) from TRMM observations [*Liu et al.*, 2008b], PFs are defined by grouping the contiguous area with the precipitation rate greater than 0.1 mm/h detected by the GPM core satellite Ku band radar. Then the properties of PFs are calculated, such as the geocenter location, horizontal area, minimum 85 GHz polarization-corrected temperature (PCT) [*Spencer et al.*, 1989], and maximum heights of 20 and 40 dBZ echo tops. Maximum 20 dBZ echo top height is one indicator of the altitude that precipitation size particles have reached in deep convective cores of precipitation systems. Maximum 40 dBZ echo top height is a proxy for the strength of the convective updraft [*Zipser et al.*, 2006]. Intense updrafts are required to lift large precipitation particles such as graupel and hail to high altitudes and are associated with lightning [*Liu et al.*, 2012] and hail [*Cecil and Blankenship*, 2012].

In total, 6.6 million PFs are defined between March 2014 and February 2015. The first release of the radar products contains some noisy signals that mostly appear as an isolated deep column of low reflectivity. There are some unrealistically small PFs having 20 dBZ echo top reaching near 20 km. To remove these noisy signals, PFs with maximum 20 dBZ echo tops greater than 17 km, but with less than four pixels ($<$80 km^2) in size and minimum 85 GHz PCT warmer than 220 K, are excluded from the samples. This sanity check leaves 6.4 million PFs that are used in this study.

3. Results

3.1. Locations of the Largest, Deepest, and Most Intense Precipitation Systems

To identify the extreme events, PFs are categorized by the top 10%, 1%, 0.1%, and 0.01% values of sizes, maximum heights of 20 and 40 dBZ echo tops, respectively. Their locations are shown with different color symbols in Figure 1. The value ranges of different categories are listed above the color scale. Because heights of 20 and 40 dBZ echo tops have values at fixed radar range bins, the categorization can only be made approximately to the selected percentages. The largest PFs with size greater than 100,000 km^2 are mostly over midlatitude and high latitude oceans (Figure 1a). We note that there are many extensive but shallow PFs over southern oceans (Figures 1a and 1b). These most likely correspond to midlatitude and high latitude cyclones occurring in all seasons, more in winter than summer (figures not shown). Consistent with the distribution of storms reaching the tropical tropopause as seen by the TRMM radar [*Liu and Zipser*, 2005], PFs with maximum height of 20 dBZ greater than 15 km are found mostly over tropical land and the West Pacific Warm Pool (Figure 1b). GPM radar also captures PFs with 20 dBZ echo above 15 km over mid-Northern U.S. and Argentina. Similar to the distribution of the strongest storms seen by TRMM [*Zipser et al.*, 2006] but with a larger global coverage by the GPM Ku radar, Figure 1c shows that the strongest PFs with 40 dBZ echo reaching above 9 km are dominant over land including midlatitude and high latitude, such as northern Europe extending across Siberian Russia and mid-Canada. Several PFs with 40 dBZ echo reaching 12 km are even found north of 60°N. Hail and lightning are expected in these systems [*Liu et al.*, 2012; *Cecil and Blankenship*, 2012].

3.2. Fraction of the Global Precipitation From Extreme Precipitation Systems

Although these extreme events are rare, they play an important role in the global water cycle. The top 0.1% of PFs by size (greater than 48,756 km^2) contribute 28% of total global precipitation (Table 1). The top 0.1% PFs by 20 dBZ echo top (greater than 14.8 km) contribute more than 10% of total global precipitation. The categorizations of PFs are analyzed for land and ocean separately in Table 2. Over ocean, the top 0.1% PFs by size are larger than those over land and contribute a larger fraction of total precipitation. Over land, for

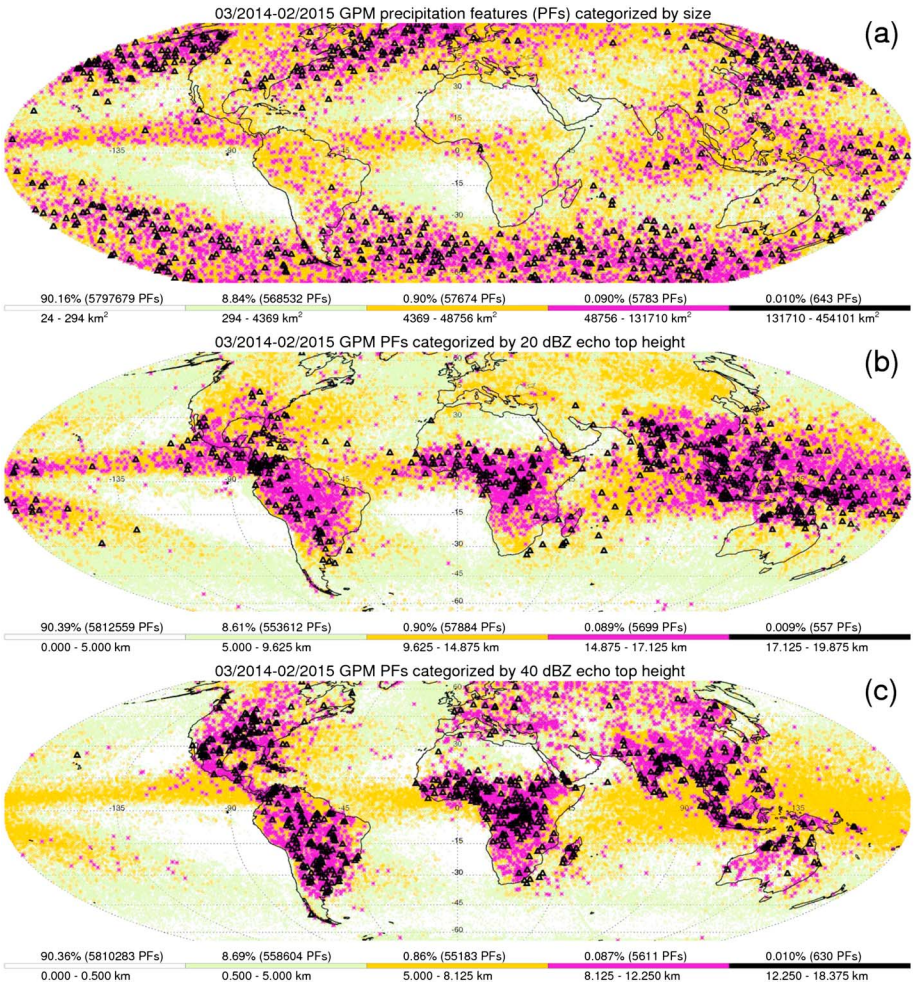

Figure 1. Locations of precipitation features (PFs) categorized by their rarity by (a) size, (b) maximum 20 dBZ echo top height, and (c) maximum 40 dBZ echo top height. The parameter limits for each category are indicated above each color bar.

each top percentage of 40 dBZ echo top, the systems are more convectively intense, although contributing a smaller fraction of total precipitation than those over ocean. For example, those with 40 dBZ echo top higher than 11 km over land (top 0.1%) contribute about 5.6% of total precipitation, while over ocean, systems with 40 dBZ echo top higher than 6.25 km (top 0.1%) contribute 13.6%.

To demonstrate the contributions of the largest PFs at different latitudes, the total global precipitation is budgeted from PFs of different sizes in 2° latitude belts and shown in Figure 2a. Figure 2a shows that large systems with size greater than 10,000 km^2 have a significant contribution (54% after accumulating the precipitation only from those large PFs) to the total precipitation. Also, from Figure 2a, more precipitation occurs in the northern hemisphere tropics than the southern hemisphere tropics in all size ranges. Consistent with Figure 1a, the PFs over midlatitude and high latitude are more concentrated in larger sizes than those over tropics. Also, these extratropical PFs are larger in winter than in summer (figure not shown). The small size systems with one top four pixels ($<$100 km^2) also have important contributions to

Table 1. Percent of Global Total Precipitation From Extreme PFs Shown in Figure 1

% Precipitation From PFs Categorized	Top 10%	Top 1%	Top 0.1%	Top 0.01%
By size (km^2)	90.8	70.0	28.4	5.6
By maximum 20 dBZ height (km)	80.9	41.7	10.4	1.4
By maximum 40 dBZ echo top (km)	82.5	42.2	6.9	1.1

Table 2. Population of Extreme PFs and Their Contribution to the Total Precipitation Over 65°S–65°N, Land, and Ocean

PFs Categorized By			Top 10%	Top 1%	Top 0.1%	Top 0.01%
Ocean	Size	Sample (#)	528,652	53,290	5,331	534
		Value (km^2)	270	3,707	49,836	136,842
		Precipitation (%)	90.6	72.1	31.0	6.22
	Max 20 dBZ echo top	Sample (#)	520,336	52,093	5,063	527
		Value (km)	4.375	8.625	14.0	16.375
		Precipitation (%)	83.3	44.6	13.8	2.5
	Max 40 dBZ echo top	Sample (#)	235,282	51,949	4,974	462
		Value (km)	0.25	3.625	6.25	8.625
		Precipitation (%)	85.1	53.1	13.6	1.6
Land	Size	Sample (#)	107,160	10,906	1,092	110
		Value (km^2)	442	7,168	44,631	102,324
		Precipitation (%)	90.3	59.8	19.7	3.7
	Max 20 dBZ echo top	Sample (#)	103,739	10,908	1,062	90
		Value (km)	7.0	12.5	16.25	18.0
		Precipitation (%)	71.4	30.4	6.0	0.9
	Max 40 dBZ echo top	Sample (#)	108,064	10,220	1,029	100
		Value (km)	2.625	7.0	11.125	15.25
		Precipitation (%)	76.5	30.0	5.6	1.0

the global precipitation, but especially over the tropics. One caveat here is that although GPM Ku radar has a little better sensitivity than TRMM precipitation radar, it still misses weak precipitation with rate <0.1 mm/h [*Hou et al.*, 2014]. Most of those weak precipitation systems are shallow and small. Therefore, it is likely that the fraction of precipitation from small systems on Figure 2a is underestimated.

Similarly, the fractions of global precipitation from PFs of different depth, in 2° latitude zones, are shown in Figure 2b. Deep PFs with 20 dBZ echo reaching above 12 km over the tropics contribute a big portion of global precipitation, although they are relatively rare (Table 2). Although there are a large number of PFs with low echo tops, their precipitation contribution is not as significant. This is consistent with past literature [e.g., *Rickenbach and Rutledge*, 1998; *Liu*, 2011]. There is a higher fraction of shallow precipitation in the southern subtropics due to the large regions of weak and shallow rainfall over area with large-scale descent (e.g., stratocumulus regions west coast of Chile and Africa). The shallow precipitation systems over southern midlatitude and high latitude have a larger precipitation contribution than their northern counterparts (Figure 2b).

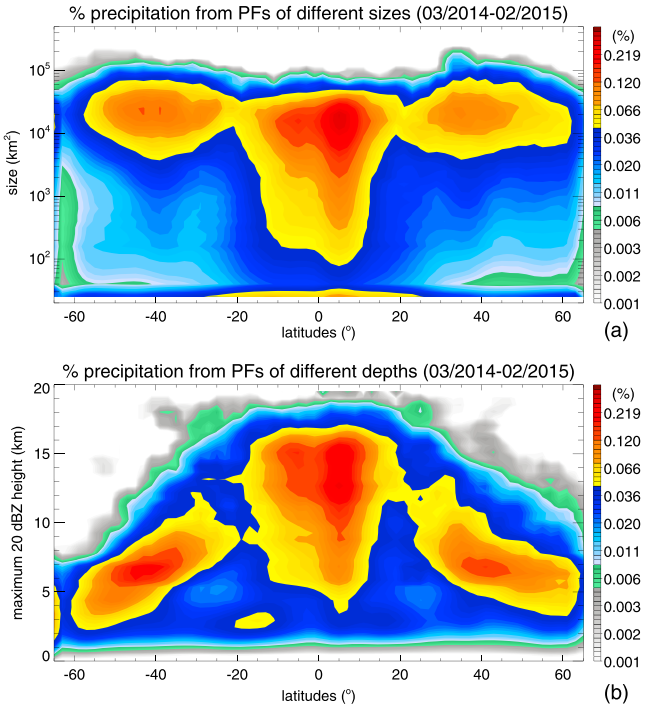

Figure 2. Contributions to global precipitation from PFs of (a) different sizes and (b) different maximum heights of the 20 dBZ echo. In both cases, the statistics are computed in 2° latitude bins. Total values add up to 100%. Note the logarithmic color scale.

4. Summary

With the first year of GPM Ku radar observations, precipitation systems of extreme size, depth, and intensity are surveyed between 65°S and 65°N. Their contributions to the global precipitation are evaluated at different latitudes. The major findings include the following:

1. The largest precipitation systems are found over midlatitude and high-latitude oceans. Notably, GPM makes

it possible to quantify the contribution of those extensive precipitation systems over midlatitude and high-latitude oceans by radar for the first time.
2. The deepest precipitation systems are most common over tropical land, the West Pacific Warm Pool, the Great Plains of the US, and Argentina.
3. The most intense storms are mostly over land. For the first time, GPM has shown that intense systems with 40 dBZ echo reaching above 10 km occur frequently at midlatitude and high-latitude locations such as northern Europe extending across Siberian Russia and mid-Canada.
4. Although the most extensive precipitation systems are rare, they have significant contribution to the global precipitation. Northern and southern midlatitude and high latitude have precipitation systems of different spectra of size and depth. There are more large and shallow systems over southern midlatitude and high latitude.

Covering more than 90% of the globe, the observations of GPM provide a full view of global precipitation. By introducing the definition of precipitation features, the budget of global precipitation from different sizes, depths, and convective intensities indicates that the extreme precipitation events contribute a significant amount in the global precipitation over different regions. This implies that it is important to describe the organization and intensity of precipitation systems in global climate models for a realistic global hydrological cycle. As more GPM observations become available, it is anticipated that various properties of precipitation systems in different regions will be explored in greater detail.

Acknowledgments

This research was supported by NASA Precipitation Measurement Mission grants NNX11AG31G under the direction of Ramesh Kakar. Thanks also go to Erich Stocker and Patty McCaughey and the rest of the Precipitation Processing System team at NASA Goddard Space Flight Center, Greenbelt, MD, for data processing assistance. All data used in this study can be downloaded from NASA website (http://pmm.nasa.gov/data-access/downloads/gpm).

The Editor thanks Svetla Hristova-Veleva and an anonymous reviewer for their assistance in evaluating this paper.

References

Cecil, D. J., and C. B. Blankenship (2012), Toward a global climatology of severe hailstorms as estimated by satellite passive microwave imagers, *J. Clim.*, *25*, 687–703.

Cecil, D. J., S. J. Goodman, D. J. Boccippio, E. J. Zipser, and S. W. Nesbitt (2005), Three years of TRMM precipitation features. Part I: Radar, radiometric, and lightning characteristics, *Mon. Weather Rev.*, *133*, 543–566.

Hou, A. Y., R. K. Kakar, S. Neeck, A. A. Azarbarzin, C. D. Kummerow, M. Kojima, R. Oki, K. Nakamura, and T. Iguchi (2014), The Global Precipitation Measurement mission, *Bull. Am. Meteorol. Soc.*, *95*, 701–722.

Houze, R. A., D. C. Wilton, and B. F. Smull (2007), Monsoon convection in the Himalayan region as seen by the TRMM precipitation radar, *Q. J. R. Meteorol. Soc.*, *133*, 1389–1411.

Kummerow, C., W. Barnes, T. Kozu, J. Shiue, and J. Simpson (1998), The Tropical Rainfall Measuring Mission (TRMM) Sensor Package, *J. Atmos. Oceanic Technol.*, *15*, 809–817.

Liu, C. (2011), Rainfall contribution from precipitation systems with different sizes, intensities and durations, *J. Hydrometeorol.*, *12*, 394–412.

Liu, C., and E. Zipser (2005), Global distribution of convection penetrating the tropical tropopause, *J. Geophys. Res.*, *110*, D23210, doi:10.1029/2005JD00006063.

Liu, C., and E. J. Zipser (2009), "Warm rain" in the tropics: Seasonal and regional distribution based on 9 years of TRMM data, *J. Clim.*, *22*, 767–779, doi:10.1175/2008JCLI2641.1.

Liu, C., E. J. Zipser, G. G. Mace, and S. Benson (2008a), Implications of the differences between daytime and nighttime CloudSat observations over the tropics, *J. Geophys. Res.*, *113*, D00A04, doi:10.1029/2008JD009783.

Liu, C., E. J. Zipser, D. J. Cecil, S. W. Nesbitt, and S. Sherwood (2008b), A cloud and precipitation feature database from 9 years of TRMM observations, *J. Appl. Meteorol. Climatol.*, *47*, 2712–2728, doi:10.1175/2008JAMC1890.1.

Liu, C., D. Cecil, E. J. Zipser, K. Kronfeld, and R. Robertson (2012), Relationships between lightning flash rates and radar reflectivity vertical structures in thunderstorms over the tropics and subtropics, *J. Geophys. Res.*, *117*, D06212, doi:10.1029/2011JD017123.

Mace, G. G., R. Marchand, and G. L. Stephens (2007), Global hydrometeor occurrence as observed by CloudSat: Initial observations from summer 2006, *Geophys. Res. Lett.*, *34*, L09808, doi:10.1029/2006GL029017.

Mohr, K. I., and E. J. Zipser (1996), Defining mesoscale convective systems by their ice scattering signature, *Bull. Am. Meteorol. Soc.*, *77*, 1179–1189.

Nesbitt, S. W., E. J. Zipser, and D. J. Cecil (2000), A census of precipitation features in the tropics using TRMM: Radar, ice scattering, and lightning observations, *J. Clim.*, *13*, 4087–4106.

Orville, R. E., and R. W. Henderson (1986), Global distribution of midnight lightning: September 1977 to August 1978, *Mon. Weather Rev.*, *114*, 2640–2653.

Rickenbach, T. M., and S. A. Rutledge (1998), Convection in TOGA COARE: Horizontal scale, morphology, and rainfall production, *J. Atmos. Sci.*, *55*, 2715–2729.

Schumacher, C., and R. A. Houze Jr. (2003), Stratiform rain in the tropics as seen by the TRMM precipitation radar, *J. Clim.*, *16*, 1739–1756.

Seto, S., T. Iguchi, and T. Oki (2013), The basic performance of a precipitation retrieval algorithm for the global precipitation measurement mission's single/dual-frequency radar measurements, *IEEE Trans. Geosci. Remote Sens.*, *51*, 5239–5251.

Spencer, R. W., and D. A. Santek (1985), Measuring the global distribution of intense convection over land with passive microwave radiometery, *J. Appl. Meteorol.*, *24*, 860–864.

Spencer, R. W., H. M. Goodman, and R. E. Hood (1989), Precipitation retrieval over land and ocean with the SSM/I: Identification and characteristics of the scattering signal, *J. Atmos. Oceanic Technol.*, *6*, 254–273.

Stephens, G. L., et al. (2002), The CloudSat mission and the A-Train, *Bull. Am. Meteorol. Soc.*, *83*, 1771–1790, doi:10.1175/BAMS-83-12-1771.

Wall, C., C. Liu, and E. Zipser (2013), A climatology of tropical congestus using CloudSat, *J. Geophys. Res. Atmos.*, *118*, 6478–6492, doi:10.1002/jgrd.50455.

Zipser, E., C. Liu, D. Cecil, S. W. Nesbitt, and S. Yorty (2006), Where are the most intense thunderstorms on Earth?, *Bull. Am. Meteorol. Soc.*, *87*, 1057–1071.